Tribology International 144 (2020) 106115

Contents lists available at ScienceDirect

Tribology International

journal homepage: http://www.elsevier.com/locate/triboint

Nanoscale frictional characterisation of base and fully formulated lubricants based on activation energy components

J. Umer [a], N. Morris [a], R. Rahmani [a,*], S. Balakrishnan [b], H. Rahnejat [a]

[a] Wolfson School of Mechanical, Electrical and Manufacturing Engineering, Loughborough University, Loughborough, Leicestershire, UK
[b] Castrol Ltd, BP Technology Centre, Whitchurch Hill, Pangbourne, Berkshire, UK

ARTICLE INFO

Keywords:
Friction
Fluid cell LFM
Fully formulated lubricant
Base oil
Activation energy
Eyring potential cage model

ABSTRACT

Tribofilms are activated using precision sliding strip microscale tribometry with a base and a fully formulated lubricant with a ZDDP anti-wear additive. The employed tribometry uses combined pressure, shear and temperature activation. The chemical compositions of the formed tribofilms are ascertained through use of Photoelectron X–ray Spectroscopy (XPS). Nanoscale frictional measurements of the tribofilms are reported using fluid cell lateral force microscopy (LFM). The measured coefficient of interfacial boundary shear strength is used with analytical contact mechanics to relate the in-situ conditions to the activation energy components of the Eyring potential cage model. The paper shows that combined LFM and the Eyring model can explain the variations in the frictional characteristics of formed tribofilms.

1. Introduction

Automotive lubricants typically comprise 85–90% base oil and 10–15% chemical additives [1], including anti-wear agents, friction modifiers, dispersants, detergents and oxidation stabilisers, as well as corrosion inhibitors [2]. Zinc dialkyldithiophosphates (ZDDP) is one of the most commonly used anti-wear additives in engine lubricants, as well as hydraulic and transmission fluids. Mechanism of ZDDP tribofilm formation is widely studied, including through hydrolytic action [3,4], thermal decomposition [5,6], catalytic surface adsorption [7] and oxidation [8]. Bovington and Dacre [7] measured the absorption and desorption of a ZDDP tribofilm on an EN31 steel surface in the presence of iron powder as a catalyst. They showed that adsorption and desorption of a tribofilm follows first order reaction kinetics, and that its associated processes are not dependent on stirring the solution. Willermaet et al. [8] studied various mechanisms and steps in the formation of ZDDP-based tribofilms on metallic surfaces. They showed that an anti-wear tribofilm forms by adsorption of ZDDP onto a surface, chemically reacting in order to form phosphothionates and phosphate-based compounds which chemically bond to the surface.

The growth of a tribofilm and its removal from metallic surfaces follows the perpetual competitive processes due to the nature of chemical reactions and wear. Watkins [4] used a highly oxidised iron surface in the presence of a ZDDP solution in order to study the mechanism of tribofilm formation on typical metallic engine components which inherit oxide layers. They showed that zinc phosphate physically adsorbs, whilst iron sulphide chemically reacts with surface materials. Furthermore, the thickness of the ZDDP tribofilm was shown to depend on various parameters, including the prevailing contact pressure, generated temperature, sliding time and shear rate [9].

The nanoscale modulus of elasticity of surfaces, including a tribofilm is another influential parameter in predicting the frictional characteristics. For nanoscale surface features, this parameter is obtained using Lateral Force Microscopy (LFM). This parameter is also one of the key parameters in defining the real (effective) area of contact. Therefore, determining the elasticity of tribofilms in physical scale of interest is quite important [10–14]. Aktary et al. [10] measured the elasticity of a ZDDP tribofilm through nano-indentation for an applied load range up to 100 μN. They produced the tribofilms by sliding a stainless-steel pin on a 52100-steel surface. The average measured nanoscale modulus of elasticity of the tribofilm was reported to be 92.6 GPa. Nicholls et al. [11] used a high frequency friction measurement instrument to generate ZDDP tribofilms on AISI 52100 steel and A319 aluminium samples. The average nanoscale modulus of elasticity was measured at the centre of the discs and reported to be 53.7 ± 14.7 GPa, whilst on the edges of the discs this value raised to 112.4 ± 18.5 GPa. Pereira et al. [12] also used a high frequency tester to analyse a wear scar on a 52100-steel sample with a ZDDP tribofilm. The test was conducted at temperatures ranging from 25 °C to 200 °C. It was observed that the measured nanoscale

* Corresponding author.
E-mail address: R.Rahmani@lboro.ac.uk (R. Rahmani).

https://doi.org/10.1016/j.triboint.2019.106115
Received 12 July 2019; Received in revised form 27 September 2019; Accepted 11 December 2019
Available online 12 December 2019

Nomenclature

A	Contact area [m^2]
C_F	Calibration factor [−]
E	Potential barrier [KJ/mol]
F_f	Friction [N]
F_N	Normal contact force [N]
E_1	Modulus of elasticity of the AFM tip material [Pa]
E_2	Modulus of elasticity of the sample surface material [Pa]
E^*	Combined modulus of elasticity [Pa]
K_B	Boltzmann constant [KJ/mol K]
P	Contact pressure [m]
Q	Activation Energy to initiate sliding [KJ/mol K]
R	AFM tip radius [m]
R_{pk}	Reduced peak height roughness
T	Operating temperature [K]
v	Sliding velocity [m/s]
v_0	Characteristic velocity [m/s]

Greek Letters

θ	Contact angle [°]
τ	Shear stress [Pa]
ν_1	Poisson's ratio of the AFM tip material [−]
ν_2	Poisson's ratio of the sample surface material [−]
μ	Coefficient of friction [−]
φ	Shear activation volume [m^3]
Ω	Pressure activation volume [m^3]

Abbreviations

AFM	Atomic Force Microscope
BO	Base oil
DMT	Derjaguin-Muller-Toporov
FF	Fully Formulated lubricant
LFM	Lateral Force Microscopy
RMS	Root Mean Square
ZDDP	Zinc dialkyldithiophosphates

modulus of elasticity was consistent up to a temperature of 150 °C, with an average value of 100 GPa. This dropped to 75 GPa when the temperature reached 200 °C. Umer et al. [13] characterised the frictional performance of various cylinder liner materials for internal combustion engine applications through LFM. The modulus of elasticity was measured through force-distance curves, using a RTESP-525 AFM probe. They measured reduced elastic modulus for the surfaces under investigation in the range 92 ± 5 GPa to 180 ± 3 GPa for the various metallic and ceramic coatings of choice for cylinder liners of internal combustion engines. Umer et al. [14] developed a methodology to characterise the tribofilm derived from fully formulated engine lubricants. The ZDDP-based tribo-film was generated on AISI 4140 steel specimen, using a precision sliding strip tribometer. They measured the combined elastic modulus of the ZDDP tribofilm to be 107 ± 7 GPa.

In lubricated sliding contacts a certain amount of energy is required for the initiation and continuance of sliding motion. The energy required for activating the reactions between the lubricant additives and the contacting surfaces can be explained through use of a thermally-activated cage model. Briscoe and Evans [15] used organic monolayers of carboxylic acid on an atomically smooth mica surface, deposited as a Langmuir-Blodgett layer [16] through dipping the mica surface into a carboxylic solution. The layer was then compressed with a load of 25 mN/m, ensuring stabilisation of a monolayer on the surface. A friction apparatus was used to measure the frictional characteristics of monolayers at various temperatures, sliding velocities and applied contact loads. They showed that fluid molecules need certain amount of energy to undergo dislocation and continuance of sliding motion relative to any neighbouring molecules. A Thermal activation cage model, based on Eyring's theory was developed to include thermal, pressure and shear components of the total activation energy. Chong and Rahnejat [17] applied the same theory to identify the relevant components of the activation theory for both base and fully formulated 10W40 lubricants on alloy steel and nickel silicon carbide samples with different surface finishes. They used an AFM probe with stiffness of 0.35 N/m and tip radius of 60 nm to measure nanoscale friction. Friction was measured in the presence of a lubricant along and across the ridges of cross-hatched honed samples, typical of cylinder liners. The nanoscale friction was measured using LFM and relative comparison of thermal, shear and pressure activation energy components of the thermally activated cage model were determined in an attempt to explain the observed frictional characteristics of the fully formulated lubricants. Ku et al. [18] also used the Eyring's activation energy model to describe measured friction of two ultra-smooth wedge pairs in relative sliding motion, entraining various fluids, including Hexadecane and Squalane.

Spikes and Tysoe [19] reported on the theoretical models developed by Prandtl-Tomlinson [20] and Eyring [21] to understand the physical phenomena associated with the boundary friction, tribo-chemistry and wear. Furlong et al. [22] developed a theoretical model, based on the Prandtl-Tomlinson model [20] to investigate the effect of temperature and velocity on sliding friction. Ewen et al. [23] studied the non-equilibrium molecular dynamic simulations of frictional characteristics of n-hexadecane on the hematite surfaces in the presence of organic friction modifiers. They investigated the effect of slip length, pressure and shear rate on the measured friction. The simulation study was carried out for shear rates of 10^8 to 10^{11} s^{-1} and showed increasing slip lengths with shear rate and contact pressure. It was also observed that the slip length is longer in the cases where the surface had high h-hexadecane coverage and that the measured friction had a strong dependence on the slip length.

Bouhacina et al. [24] studied the nanoscale frictional characteristics of silica wafers, 3-Ethoxysilane grafted on silica wafer and polyacetylene grafted on 3-ethoxysilane, using LFM at sliding velocities in the range 10^2 to 10^4 nm/s. They used three AFM probes with spring constants of 0.12, 0.58 and 0.38 N/m respectively. They also used the Eyring model to interpret their measured friction results and determine the Eyring parameters. The characteristic velocity and shear activation volume were estimated to be 100 m/s and 0.2nm^3 respectively for all the samples. The barrier height and shear strength of the samples were estimated and their dependence on the sliding velocity and activation volume were determined. Additionally, the Eyring energy parameters were shown to be independent of the nature of the AFM probes used in the study. Müser [25] also studied the dependence of measured friction on the velocity and temperature using the Prandtl-Tomlinson (PT) model [20]. The molecular dynamic simulation was used to numerically solve the Langevin equation for the PT model for up to 6th order of the sliding velocity and 2nd order of temperature variation. They observed that the transition in friction from a linear variation to the Coulombic type occurred at intermediate temperatures. The results indicated that friction has strong dependency on sliding velocity at higher temperatures, but variation of friction with velocity is negligible at low temperatures. Fusco and Fasolino [26] investigated the atomic scale friction and its dependence on the sliding velocity in 1-D and 2-D Tomlinson models. They studied the effect of damping (AFM probe), dimension (1 and 2 D), and temperature variation (athermal and finite temperature) on friction-sliding velocity relationship. The effect of damping was found to be important at higher velocities, indicating the variation of atomic scale slip on number of lattice points affecting the measured

friction.

The above review of literature shows that most studies have been concerned with experimental measurement of the effect of governing parameters such as shear rate, contact temperature and applied pressures upon the formation of a tribofilm, with particular emphasis on ZDDP and MoS2 and their variants (as discussed above). Hitherto, a comprehensive friction model does not exist which would allow for prediction of friction of adsorbing/desorbing tribofilms on various surfaces. The Eyring activation model [21], based upon the transition state theory and physio-chemical principles provides a good means of relating measured shear/frictional characteristics to adsorption of boundary active additives through determination of energy barriers for activation. The current study characterises engine lubricants' frictional behaviour at nanoscale using the Eyring's activation energy concept. A base oil (BO) and a fully formulated (FF) lubricant are used in the study. A tribofilm is activated and formed on the specimen surfaces through mechanical activation, using a precision sliding strip tribometer. Subsequently, LFM is used in the presence of a lubricant (wet LFM) to measure the nanoscale surface friction. Eyring energy thermal activation model is integrated with a contact mechanics model to understand the boundary film behaviour for both BO and FF at various applied normal loads and sliding velocities. Pressure, shear and thermal activation energies in the Eyring energy model are shown to vary with the test conditions, primarily due to the nature of the molecules within the sliding contact.

2. Theoretical model

The theoretical model comprises a contact mechanics model to predict the expected contact stresses, which are required to determine the activation energies and associated parameters for the Eyring activation model as highlighted by Briscoe and Evans [15].

2.1. Contact mechanics

To determine the area of contact for the LFM measurements, an appropriate contact mechanics model is required. The contacts with non-negligible adhesive component have been studies by Bradley [27], Derjaguin et al. [28], Johnson et al. [29] and Maugis [30]. Those with negligible adhesion are broadly dealt with the classical Hertzian theory [31]. With the presence of lubricant in wet LFM tests reported here, the work of adhesion is negligible, and use of classical Hertzian theory is upheld. The adhesion map of Johnson and Greenwood [32] is used to determine the appropriate contact mechanics theory for the wet LFM tests (noted as BO and FF points in Fig. 1). The load parameter ($\overline{P}$) is the ratio of applied normal load to the measured adhesive force at the AFM tip surface conjunction: $\overline{P} = \frac{F_N}{\pi w R}$, where, F_N is the applied normal load, w is work of adhesion and R is the tip radius. The Tabor or elasticity parameter (λ) is given as: $\lambda = 1.16\left(\frac{Rw^2}{E^{*2}z_0^3}\right)^{1/3}$, where E^* is the combined elastic modulus, and z_0 is the atomic separation at equilibrium. The force of adhesion, measured through the force-distance curve for the BO and FF lubricants samples are 0.07 nN and 0.04 nN respectively. The subsequent values for the work of adhesion (w) for the BO and FF lubricant samples are 3.47×10^{-4} J and 2.07×10^{-4} J respectively. The values for atomic separation at equilibrium (z_0) is considered to be 0.4 nm in the range discussed by Jacob et al. [33]. The load parameters measured for the base and fully formulated oil samples were 4.17×10^3 and 6.28×10^3 respectively. The corresponding calculated elasticity parameters are 1.78×10^{-3} for the base oil (BO) and 1.26×10^{-3} for the fully formulated lubricant (FF) samples for the experimental conditions for the fluid cell (wet) LFM. Fig. 1 shows that with the presence of both fluids, Hertzian contact mechanics can be used, thus:

$$A = \pi\left(\frac{3RF_N}{4E^*}\right)^{2/3} \tag{1}$$

where, R is the radius of the tip of the AFM probe, F_N is the normal applied load and E^* is combined (reduced) modulus of elasticity of the sample and the silicon nitride tip [34]:

$$E^* = \left(\frac{1-\nu_1^2}{E_1} + \frac{1-\nu_2^2}{E_2}\right)^{-1} \tag{2}$$

The average shear stress and contact pressure are obtained as:

$$\tau = \frac{F_f}{A} \tag{3}$$

$$P = \frac{F_N}{A} \tag{4}$$

Fig. 1 also shows 2 measurement points for dry pre and post tribometry samples, described in subsection 3.4. In both cases, the DMT contact mechanics theory is used.

The procedure to measure the modulus of elastic of the sample surface for both pre-tribometry virgin samples and post tribometry samples with an adsorbed tribo-film layer is described in subsection 3.4.

2.2. Eyring activation potential cage model

Interaction of contiguous surfaces in boundary regime of lubrication can be explained through the activation energies which overcome a cage-like potential barrier as shown in Fig. 2. The average time required for a single molecule to overcome this potential barrier is assumed to conform to a Boltzmann distribution [21]. The barrier is present due to the interactions with the neighbouring molecules. All molecules need to overcome this energy barrier for any dislocation and subsequent

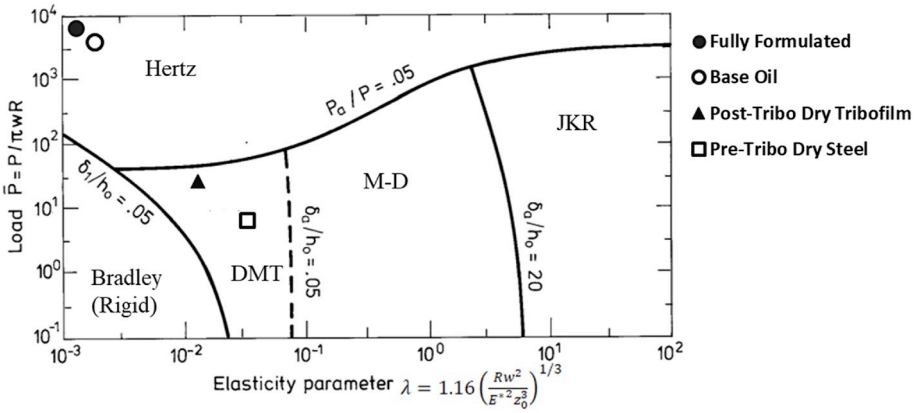

Fig. 1. The test conditions for wet LFM within the adhesion map.

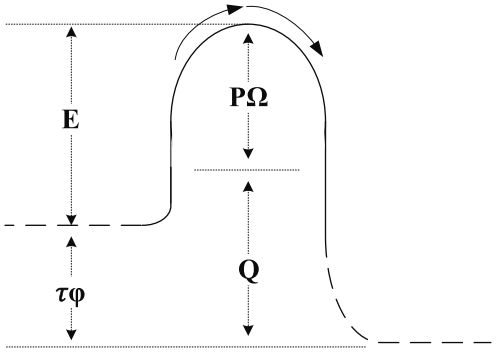

Fig. 2. Schematics of thermally activated energy barrier.

continuance of motion. The energy barrier is overcome due to prevailing temperature and generated contact pressures and shear [15].

The potential barrier; E with the components of activation energy to initiate sliding; Q, and contributions due to generated pressures; $P\Omega$, and shear; $\tau\varphi$ can be described as:

$$E = Q + P\Omega - \tau\varnothing \tag{5}$$

where, Ω and φ are pressure and shear activation volumes, respectively. The contact pressure, P increases the barrier potential, but shear reduces the effort required for relative sliding of contacting solids. These activation energy components in the sliding motion would increase or decrease with respect to the state of thermodynamic equilibrium and can result in either positive or negative components of pressure and shear activation energies [15,17,35–37]. The Eyring shear stress associated with energy barrier components can be described by Refs. [15, 17]:

$$\tau\varnothing = K_b T \ln\left(\frac{v}{v_0}\right) + (Q + P\Omega) \tag{6}$$

where, K_b is the Boltzmann constant, T is the operating temperature and v is the sliding velocity. v_0 is a characteristic constant velocity with a value of 20 m/s. This is estimated from the product of molecules vibrational frequency (about 10^{11} s^{-1}) and the lattice constant (0.2 nm). The calculation of Eyring energy parameters is quite insensitive to the estimated value for the characteristic velocity as discussed by Briscoe and Evans [15]. The dependency of the barrier cage model on the variation in estimated characteristic velocity is quite insignificant [15, 24]. Furthermore, the shear stress can be described as a function of sliding velocity and contact pressure for an isothermal case as [15,38]:

$$\tau = \tau_0 + \frac{\Omega}{\varnothing} P \tag{7}$$

$$\tau = \tau_1 + \frac{K_b T}{\varnothing} \ln v \tag{8}$$

where:

$$\tau_0 = \frac{1}{\varnothing}\left[K_b T \ln\left(\frac{v}{v_0}\right) + Q\right] \tag{9}$$

and:

$$\tau_1 = \frac{1}{\varnothing}[Q + P\Omega - K_b T \ln v_0] \tag{10}$$

These are the shear stress components at constant pressure and sliding velocity respectively.

The coherence length using the shear stress activation volume is determined as [39]:

$$l = \frac{\varphi}{A} \tag{11}$$

where, A is the Hertzian contact area. Using the graph representing the measured friction against logarithm of sliding contact velocity, using the best linear fit to the associated data, it is possible to determine the slope $((K_b T/\varnothing)$ in equation (8). This slope is further used to find the shear activation volume with known values of Boltzmann constant, K_b and contact temperature, T. Then, equation (7) is used to find the slope $\Omega/\varnothing$, which is essentially the gradient of shear stress-contact pressure variation. This slope is then used to determine the pressure activation volume Ω using the already obtained value for the activation shear volume. The slope $\Omega/\varnothing$ in equation (7) is related to the coefficient of friction by the relationship [40]:

$$\mu = \tau_0/P + \Omega/\varnothing \tag{12}$$

Finally, the required activation energy for the sliding motion; Q, is determined, using equation (9).

3. Experimental investigations

This section provides the specifications for the lubricant and specimen surfaces as well as the procedure for activation of lubricant additives and the formation of a tribofilm through tribometry. The lateral force microscopy (LFM) is also used to determine the nanoscale friction as well as the modulus of elasticity of various sample surfaces, including any formed tribofilm layers.

3.1. Preparing the samples

The sample used for all the flat specimens is made of AISI 4140. A base oil (BO) without the presence of any additive, as well as a typical fully formulated 5W30 engine lubricant (FF) are used for the various tribometer tests. The elemental composition of the lubricant formulation is given the in Table 1 and the rheological properties for the base oil and the fully formulated lubricant are provided in Table 2.

3.2. Generation of adsorbed layers through tribometry

A precision sliding strip tribometer (Fig. 3) is used, where a thin strip (D) with a contact face profile representing a typical piston compression ring is loaded (H) against a flat specimen surface (E) and slides via a precision backlash free leadscrew (B) relative to it. The generated contact pressures and sliding velocity (via an electric motor, A) are representative of the prevailing conditions at the top dead centre reversal of high-performance race engines in transition from the compression to power stroke. The contact of the sliding strip with the flat specimen is lubricated, with the specimen attached to a floating plate (C). The inertial dynamics of the floating plate is resisted by contact friction, which is measured by high precision piezoelectric sensors (F). The encoder (G) provides precise measurement of travelled distance by the loaded strip. More detailed description of this tribometer is provided elsewhere [41, 42].

Friction measurement was conducted at room temperature after thorough cleaning of all the samples and the sliding strip counter faces. 2 ml of lubricant was applied onto the surface of the specimen and 40 reciprocating strokes of the strip were conducted for each test. The purpose of using this limited number of strokes was to avoid any notable change in the surface topography of the specimens through wear.

Table 1
Main elemental composition of the fully formulated 5w30 lubricant.

Elements	Concentration [ppm]
Sulphur	2600
Calcium	1980
Zinc	900
Phosphorus	780

Table 2
Rheological data for the lubricant samples.

Lubricant Sample	Parameter	Values
Base oil	Density at 15 °C	0.835 ± 0.001 g/ml
	Kinematic viscosity at 40 °C	19.7 ± 0.1 cSt
	Kinematic viscosity at 100 °C	4.3 ± 0.1 cSt
5W30 lubricant	Density at 15 °C	0.846 ± 0.001 g/ml
	Kinematic viscosity at 40 °C	52.1 ± 0.1 cSt
	Kinematic viscosity at 100 °C	9.5 ± 0.1 cSt

Table 3 lists the salient operating conditions. The procedure is further explained in Ref. [14].

3.3. Lateral force microscopy (LFM)

Nanoscale friction was measured at the asperity scale using a Veeco Dimension 3100 atomic force microscope (AFM), operating in lateral force mode (LFM, Fig. 4) [43–50] in the presence of lubricant. The AFM tip was contained in a fluid cell, keeping the inlet meniscus sufficiently far away from the tip to guard against any capillary adhesion (Fig. 4).

Friction was measured in lateral force mode using the trace minus retrace (TMR) method, where the AFM tip is scanned in the direction perpendicular to the tip cantilever [43]. The tip radius was characterised before each friction measurement by scanning a sample of known topography (TGT1: NT-MDT). The TGT1 characteriser is a Silicon wafer grating of sharp featured tips with 0.3–0.5 μm heights in periodic spacing of 3 μm. The AFM probe used for the measurement is scanned on the TGT1 grating, using a scanning area of 10 × 10μm^2 with a very slow scanning frequency of 0.25 Hz. Subsequently, the AFM tip radius is measured, based on the height image generated by the TGT1 grating. Each measurement was conducted with a new calibrated tip, using the blind calibration approach, highlighted in Refs. [49,50]. A mono-crystalline Si_3N_4 sample with the known coefficient of friction of 0.19 [17,47,50] is used to calibrate the tip frictional response. Lateral force measurements were conducted over a scan area of 1× 1μm^2 with DNP-10 tip-B, having a nominal spring constant of 0.12 N/m. The area is initially scanned under dry conditions and thereafter, the lubricant was carefully added to the contact. The average surface roughness and the root mean square roughness were measured for the AISI 4140 steel sample before LFM under nominally dry contact conditions to be 6.78 ± 0.87 nm and 8.77 ± 1.13 nm respectively. Although it is anticipated that the evaluation of Eyring energy parameters presents a combined effect of the surface roughness and molecular motion, the effect of surface roughness on the variation in the activation energy components is deemed to be insignificant as surfaces with similar topographies are used for both lubricant types. A wet-AFM holder was used with sufficient lubricant carefully added to the tip-sample interface in order to maintain a meniscus around the tip holder. This keeps the capillary forces away from the scanned area [51]. The controlled ambient conditions (20 ± 2 °C and 50 ± 5% RH) were maintained for all the experiments. The calibration factor, C_F, was determined for the tip using [49,50]:

$$C_F = \frac{F_f[\mathrm{V}]}{F_N[\mathrm{nN}] \times 0.19} \tag{13}$$

where the measurements in voltage output are converted to *nN*.

The measured data was curve-fitted with the best polynomial fit to determine the calibration factor. This factor provides the response of the AFM tip in use. Friction is then determined for any sample using:

$$F_f[nN] = \frac{F_f[V]}{C_F} \tag{14}$$

The maximum standard error for the AFM/LFM measurements, conducted on the current set up of the Veeco dimensional 3100 AFM has already been reported to be negligible previously for both dry and wet LFM with values of 0.9 nN [13] and 0.4 nN [14] respectively.

As sharp changes in local surface topography can affect the nanoscale frictional measurements, experiments for each sample were carried out in a number of locations. Furthermore, care was taken to select areas for LFM through initial topographical measurements (Fig. 4) in order to avoid, as far as possible, any sharp contours/undulations.

3.4. Nanoscale elasticity

Clearly, post-tribometry a tribo-film is formed on the surface of the samples, when the fully formulated lubricant is used. The modulus of elasticity of the tribo-film is clearly not that of the parent virgin steel substrate. Measurement of this modulus of elasticity of the sample surfaces with a tribofilm is required in order to use the Hertzian contact

Table 3
Parameters for slider rig tribometer testing.

Parameters	Values [units]
Sliding speed	(13.0–27.0) ± 0.2 [mm/s]
Load	777 ± 9 [N/m]
Stroke Length	23.0 ± 0.1 [mm]
Width of sliding strip	32.00 ± 0.01 [mm]

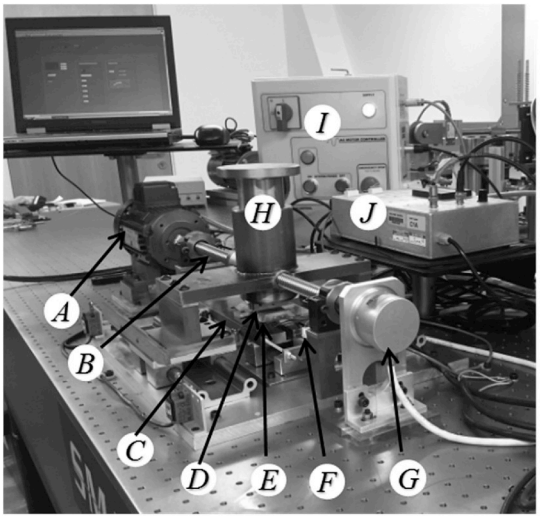

A. Electric motor
B. Lead screw
C. Floating plate
D. Sliding strip
E. Flat sample
F. Piezoelectric sensor
G. Encoder
H. Applied load
I. Motor controller
J. Force transducer amplifier

Fig. 3. The sliding strip tribometer to generate and characterise the tribo-film.

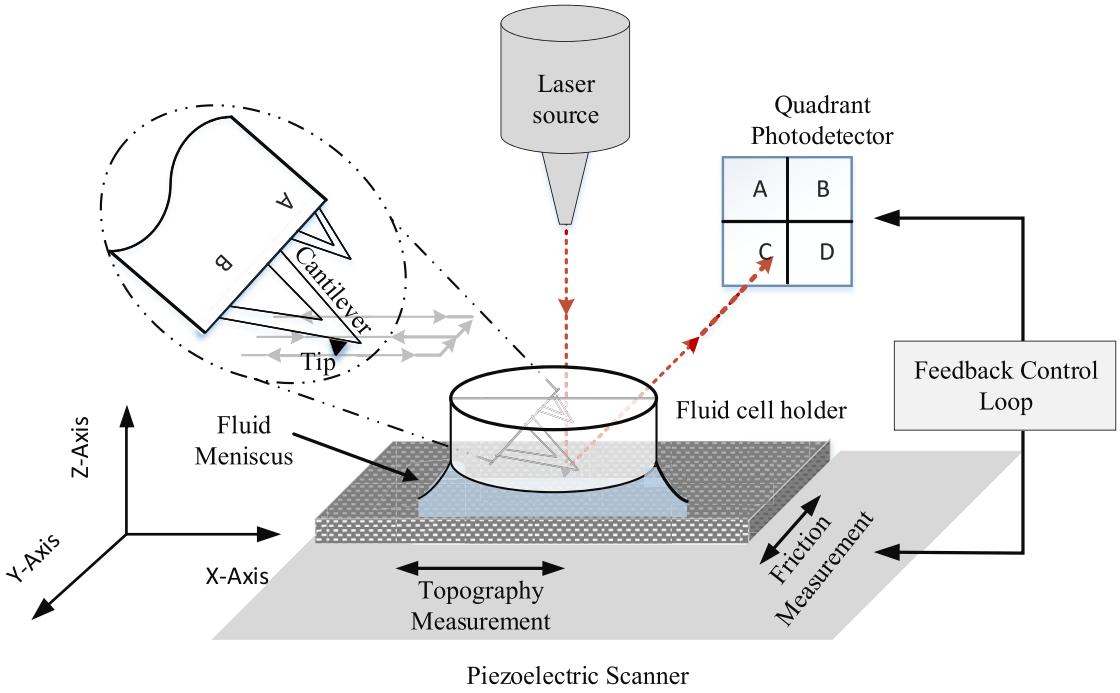

Fig. 4. Nanoscale frictional measurement using wet LFM.

theory described in section 2.1 (equation (1)). This localised elastic modulus is measured by a force-distance curve, which is subsequently used in the Eyring energy activation model. The elastic modulus is measured for each sample under dry contact condition, post tribometry and after the removal of the lubricant using petroleum ether and subsequent atmospheric drying of the surface. Therefore, the sample surfaces only comprise any tribo-film layers. To determine the nanoscale modulus of elasticity of the sample surfaces for the range of desired normal loads, force-distance (FD) curves created using AFM measurements are analysed. The elastic modulus measured through the FD curve presents the material elasticity at a normal load of a few hundred nN. It should be noted that a conventional nano-intender measures the modulus of elasticity at normal loads much higher than this range of applied loads [13,14,44], but includes the reaction of substrate material as well as any overlaid tribo-film, therefore the measurements cannot be confined to the tribofilm layer in the case of nano-indentation methods. The FD curve using LFM, however, is created for the outermost layer of the surface, ideally only for any formed tribofilm layer. A tip with a cantilever stiffness of 200N/m is used for this purpose. Clearly under dry contact conditions both the virgin sample and the post tribometry samples with a tribo-film exhibit a certain degree of adhesion as shown in Fig. 5 force-displacement traces. The load parameters measured for the pre tribotest dry steel and post tribotest dry tribofilm surfaces are 5.19 and 20.8 respectively. The corresponding calculated elasticity parameters are 3.11×10^{-2} for the pre-tribotest dry steel and 1.23 $\times$ 2 for post tribotest dry tribofilm for the dry force-distance analysis (Fig. 5). The relevant values of load parameters and elasticity parameters for the both pre tribotest dry steel and post tribotest tribofilm, with the measurement points shown in the adhesion map of Fig. 1 resides in the DMT region. Therefore, nanoscale modulus of elasticity is determined using the DMT theory.

The pull-off force in the retraction force-distance curve (Fig. 5) shows the presence of adhesion in the dry measurements through use of tip B of DNP 10. The pull-off force measured for the case of the tribo-film is less than that of the virgin steel samples (pre-tribometry). N/ m Precise measurements were carried out for the purpose of measuring elastic modulus of surface with a stiff RTESP-525 rectangular tip (k = 200 N/ m) for both cases to reduce the effect of the cantilever stiffness over a

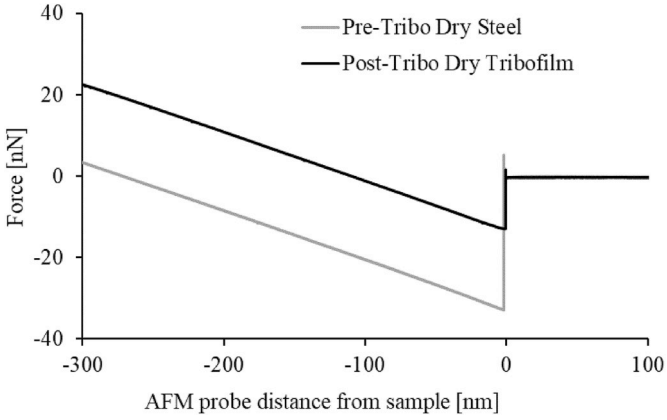

Fig. 5. Dry LFM-measured force-distance curves for virgin samples and those with a tribo-film.

large range of samples. The results show a combined (reduced) modulus of elasticity of 121 ± 6 GPa for virgin steel samples against the silicon nitride tip (equation (2)) and 107 ± 7 GPa for all samples with a formed tribofilm. The details of the measurement procedure can be found in Refs. [13,14].

4. Results and discussion

The fluid cell lateral force microscopy (wet LFM) is conducted with the lubricated samples after the formation of a ZDDP-based tribofilm activated through tribometry. The experimental methodology for the formation and characterisation of ZDDP tribo-film is briefly explained in section 3.2 and in detailed elsewhere [14]. The tribometer also incorporates a floating plate upon which the lubricated sample is mounted. The assembly is drag by the sliding strip, the inertial dynamics of which is resisted by contact friction. In this manner the piezoelectric load cells directly measure friction. The measured friction traces for the cases of base oil (BO) and fully formulated lubricant (FF) are shown in Fig. 6. The average value of coefficient of friction for the fully

formulated lubricant is observed to be higher than that for the base oil by a factor of 0.02. This increase in friction is due to the formation of a ZDDP-derived tribo-film as also noted in Ref. [14]. The presence of bonded elements as constituents of the activated tribofilm on the steel sample surfaces is ascertained by removing the hydrocarbon residue through a standard cleaning process using petroleum ether. X-ray Photoelectron spectrometry (XPS) is used for elemental analysis of the tribofilm layer for samples using base oil or the fully formulated 5W30 lubricant as shown in Fig. 7. The presence of Zn2p3, S2p, P2p in the XPS analysis for the post tribotest for fully formulated lubricant in Fig. 7 shows the generation of a ZDDP-based tribofilm on the surface through tribometry, in line with the findings of [14,52,53]. The presence of calcium in the tribofilm shows the formation of calcium-based detergent tribofilm on the surface in line with [54,55].

The fluid cell LFM results for the base and fully formulated lubricant samples are shown in Fig. 8. The results shown are for tip sliding velocities in the range 2.5–20 μm/s and at an applied normal load range of 18–40 nN (equivalent to a Hertzian contact pressure of 3.3–4.1 GPa). The normal loads are different for both lubricants due to the blind calibration technique adopted for LFM as explained in section 3.3. The average tip radius measured through the TGT1 calibrator was 22 nm for the LFM analyses. The measured friction results show that at all the tested sliding speeds, the fully formulated lubricant generates higher friction with relatively similar contact loads. This can be attributed to the existence of anti-wear additives such as ZDDP in the fully formulated lubricant, which was examined through XPS and also noted in Refs. [14, 52,53].

The shear stress is obtained, based on the results in Fig. 8 considering a Hertzian contact area, as explained in section 3.3. The variation of shear stress with speed at different normal loads is shown in Fig. 9.

The nanoscale modulus of elasticity of the tribo-film and steel sample were measured with the procedure highlighted in section 3.4. The calculated combined (reduced) elastic modulus for the sample and the tribofilm is listed in Table 4. The measured elastic moduli are used to calculate the Hertzian contact area in each case and subsequently determine the generated contact pressures and shear stresses from the LFM measurements using equations (3) and (4), respectively.

Note that the elastic modulus of the AFM tip monocrystalline Si_3N_4 sample is 310 GPa with a Poisson's ratio of 0.2 (for equation (2)).

The coherence length, determined through equation (11), is shown for the tested loads and for both base and fully formulated lubricants in Fig. 10. The coherence length represents either the length of a liquid segment, molecules or a dislocation which translates through the sliding process. In this process, a low entropy boundary layer forms on the surface through structuring of the liquid segments [15,18]. The negative values for the base oil are due to a decreasing trend in shear stress with increasing sliding velocity for the base oil, resulting in a negative slope. However, the fully formulated oil exhibits a rising shear stress with increasing sliding velocity. To quantify these, the absolute values of coherence length are considered to compare the lengths for both the base and fully formulated lubricants. The results in Fig. 10 show a clear rise in stress activation length with contact pressure for the base oil and the fully formulated lubricant. The higher contact pressures cause long hydrocarbon chains to stretch and align with the sliding direction, resulting in a higher value of coherence length. This can also be explained on basis of shear-induced ordering of molecules at the sliding interface [56]. For the fully formulated lubricant and in the presence of ZDDP and other additives, the coherence length is shorter due to shorter molecular chains present during polymerisation and depolymerisation processes as explained in Ref. [57]. In this process the ZDDP-based tribofilm formation involves depolymerisation, in which the phosphate chain length decreases to attain highly negative charge required to exchange Fe^{3+} with the Zn^{2+} ions and balance the reaction for the polymerisation process. This results in the formation of zinc-phosphate layer, overlaid by a mixture of short and long chain phosphate glass [57]. The result for the fully formulated lubricant is shown in Fig. 10.

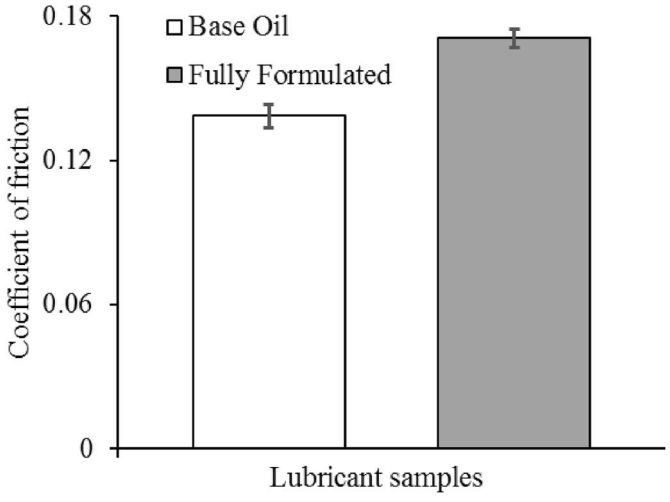

Fig. 6. Average tribometric measured coefficient of friction for the base oil and the 5W30 fully formulated lubricant.

The parameters for the thermally activated cage model [15,16] are determined, following the procedure highlighted in section 2.2. The characteristic velocity, $v_0 = 20$ m/s is used for both lubricant types. The shear and pressure activation energies, the energy to initiate the sliding motion and the energy barrier heights for the base and fully formulated lubricants are shown in Fig. 11.

Shear activation energy can be associated with the energy required to initiate sliding motion. As it can be seen from Fig. 11a, the overall shear activation energy remains relatively constant within the sliding velocity range considered in the current study for both the base and fully formulated lubricants. Furthermore, for the base oil, the shear contribution to the overall energy decreases with contact pressure (Fig. 11a) but remains negative for all the tested loads. This negative value of shear activation energy represents the presence of higher surface energy of adhesion [17,35]. The shear activation energy decreases with increasing contact pressure, thus indicating an increase in surface energy at higher loads due a decrease in separation between AFM tip and sample surface.

The shear activation energy remains positive for fully formulated lubricant due to a reduction in the surface energy [58] because of the ZDDP-based tribofilm formation. However, the response of shear activation energies for the fully formulated lubricant shows a rise with contact load. This can be interpreted as a decreased potential because of reduced surface energy by ZDDP-based tribofilm with increasing normal loads.

The pressure activation volume, Ω, can be linked to the local increase in volume, because of molecular motion [15,17]. However, the pressure activation energy is defined as the energy associated with the molecules' ability to withstand applied load. This can be interpreted as the load bearing ability of the boundary film lubrication. The lubricants with higher load bearing capacity form thicker layers boundary films, which would increase separation of sliding surfaces and reduce surface energy [26]. The pressure activation energy values for the fully formulated lubricant show a slight increase in magnitude with rising sliding velocity. This indicates the effect of additives in organisation of lubricant molecules and perhaps the transition from boundary to hydrodynamic regime of lubrication in the confined AFM tip -sample surface conjunction [18,59]. In case of fully formulated lubricant, the pressure activation energy is increasing with the normal load, forming a better boundary layer in presences of ZDDP-based tribofilm at higher loads [31]. The pressure activation energy is negative for the base oil at all the tested loads and sliding velocities. The load bearing ability of the base oil is quite poor due to an insufficient decrease in the surface energy. Furthermore, the pressure activation energy is more negative with an increase normal load. This is due to the AFM probe becoming closer to

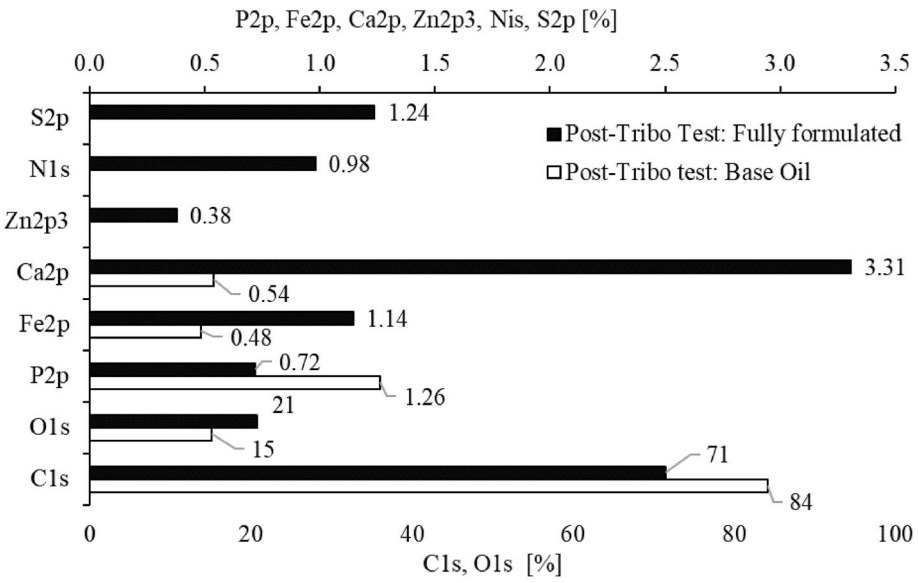

Fig. 7. XPS analysis of the steel sample surfaces after tribo-film activation through slider rig tribometry with base and fully formulated oils.

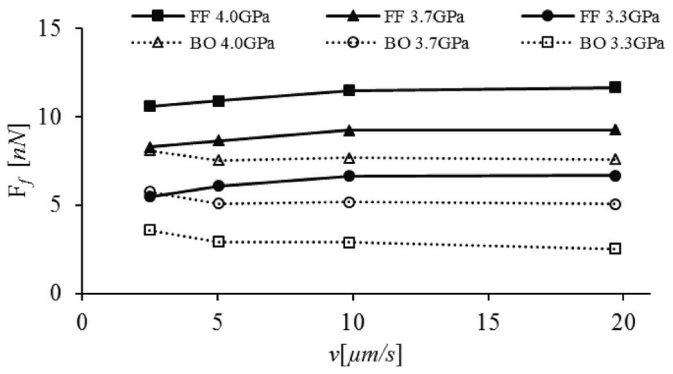

Fig. 8. Measured friction for base and fully formulated lubricants on steel sample surfaces at various normal loads and sliding speeds; FF: Fully formulated, BO: Base oil.

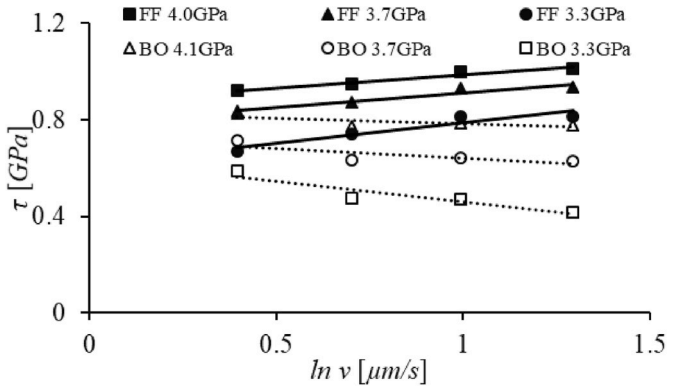

Fig. 9. Shear stress variation with the logarithm of sliding velocity for different applied normal loads for both the base and fully formulated lubricants; FF: Fully formulated, BO: Base oil.

the sample surface owing to poor load carrying capacity of the base oil. Therefore, higher surface energy and adhesion occurs at higher applied loads in the case of base oil (Fig. 11b).

Energy required to initiate and continue sliding; Q shows a decreasing trend with sliding velocity for both the base and fully formulated lubricants (Fig. 11c). Generally, higher values of Q are observed for the fully formulated lubricant. This can be attributed to the presence of ZDDP molecules in the fully formulated oil, which results in higher frictional resistance at molecular level, and hence the requirement for more energy to initiate and continue the sliding motion [1,14,16]. The energy required for sliding in the fully formulated lubricant conjunction is relatively insensitive to the applied normal load. However, for the base oil a decreasing trend for Q with the normal load is

Table 4
Combined (reduced) moduli of elasticity determined through force-distance curves of LFM.

Combined (reduced) elastic modulus (E^*)	Value [GPa]
Steel sample with no tribofilm (Pre-tribotest)	121 ± 6
Steel sample with Tribofilm (Post tribotest)	107 ± 7

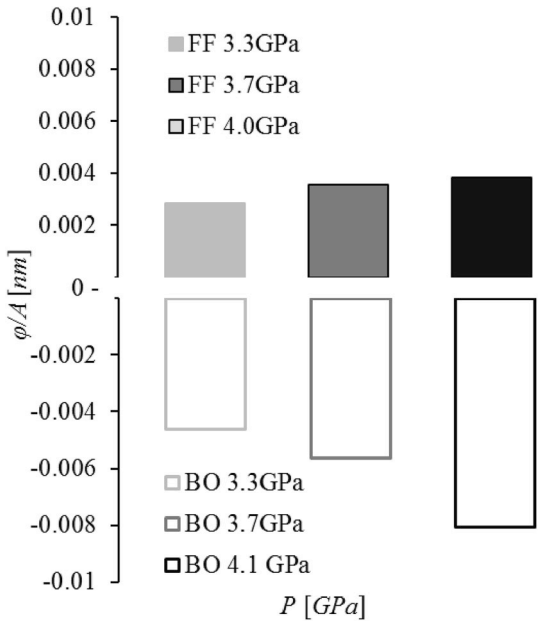

Fig. 10. Stress activation length for fully formulated and base lubricants.

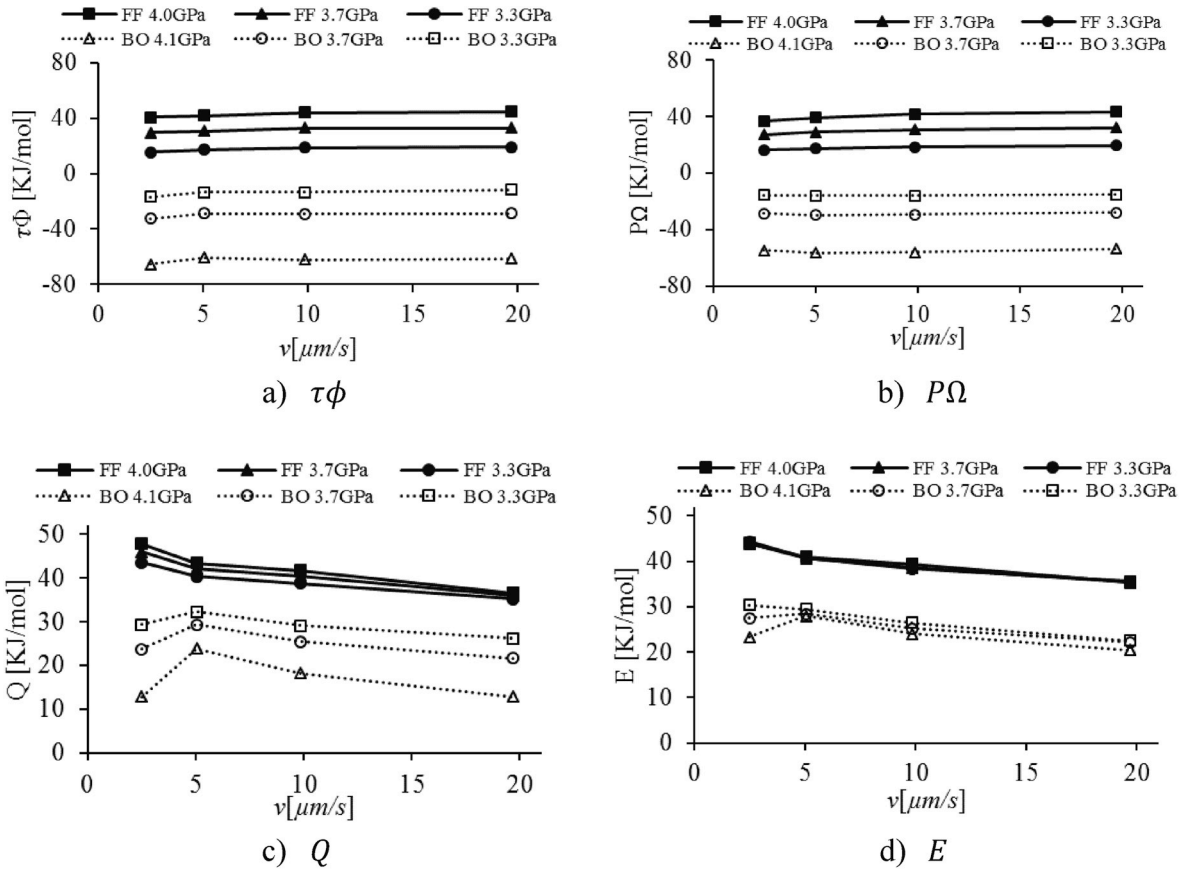

Fig. 11. Eyring energy parameters: a)$\tau\varphi$, b)PΩ, c)Q and d)E at various loads and sliding velocities.

observed. This can be explained by the coherence length as discussed in the Fig. 10. As the coherence length increases with the contact load, hydrocarbon chains become restructured (stretched) [56]. As the result, the energy required to continue sliding for the base oil molecules is less at higher loads. Finally, the results for energy barrier height, *E*, are shown in Fig. 11d. The energy barrier has shown generally a decreasing trend with the sliding velocity for both base and fully formulated lubricants. The energy barrier height for fully formulated lubricant is higher for all the tested loads than for the base oil. This shows that the presence of a ZDDP-based tribo-film increases the energy barrier height.

5. Conclusions

In the current study lateral force microscopy (LFM) is used to evaluate the frictional characteristics of a base oil and a typical fully formulated 5W30 engine lubricant. The sliding strip triobmetric tests are carried out on AISI4140 steel samples to produce an adsorbed layer of ZDDP-based tribofilm derived from the fully formulated 5W30 lubricant. Measured friction is shown to be higher in the presence of the fully formulated 5W30 lubricant due to the presence of a ZDDP-based tribofilm formed on the sample surfaces, as quantified by XPS elemental analysis. The results are explained, based upon an interpretation of the Eyring potential cage model. For this purpose, the associated energy parameters are calculated at different contact pressures and sliding velocities. The coherence length derived from the shear activation volume for the base oil is shown to be larger than that for the fully formulated lubricant, possibly due to the presence of shorter chain lengths of Fe/Zn.

The shear and pressure activation energy parameters do not change significantly with increasing rate of sliding but alter with the applied normal load to a certain extent. The base oil exhibits negative values of pressure and shear activation energies, which is an indication of higher residual surface adhesion. The fully formulated lubricant exhibits positive values for the shear and pressure activation energies, thus forming a better boundary layer of ZDDP- based tribo-film than the base oil. This also shows that the fully formulated lubricant provides better load carrying capacity in comparison to the base oil. The energy required to initiate and sustain sliding motion is shown to be higher for the fully formulated lubricant. The energy barrier height is observed to be higher in the case of fully formulated lubricant due to the presence of a ZDDP-based tribofilm. Thus, the observed values of higher friction at microscale in slider rig tribometry and nanoscale in fluid cell LFM [3,14] can be associated with the ZDDP-based tribofilms as shown in the Fig. 11d.

Acknowledgements

The authors would like to express their gratitude for the financial support of the Engineering and Physical Sciences Research Council (EPSRC) and BP through Centre for Doctoral Training in Embedded Intelligence (CDT-ei). The first Author also acknowledges the financial support provided to him by the University of Engineering and Technology Lahore under the faculty development programme to conduct this research at Loughborough University. The authors also acknowledge the use of facilities within the Loughborough Materials Characterisation Centre (LMCC).

References

[1] Zhang J, Spikes HA. "On the mechanism of ZDDP antiwear film formation". Tribol Lett 2016;63(2):24.
[2] Rudnick LR. Lubricant additives: chemistry and applications. second ed. Boca Raton: CRC Press Taylor & Francis Group; 2009. 2009.
[3] Spedding H, Watkins RC. The antiwear mechanism of ZDDP's, Part I. Tribol Int 1982;15(1):9–12.
[4] Watkins RC. The antiwear mechanism of ZDDP's. Part II. Tribol Int 1982;15(1): 13–5.

[5] Sung-H C, Ludema KC, Potter GE, Dekoven BM, Morgan TA, Kar KK. A model of the dynamics of boundary film formation. Wear 1994;177(1):33–45.
[6] Barkshire IR, Prutton M, Smith GC. Multi-spectral scanning Auger microscopy of tribological surfaces. Appl Surf Sci 1995;84(4):331–8.
[7] Bovington CH, Dacre B. The adsorption and reaction of decomposition products of zinc di-isopropyldiophosphate on steel. ASLE Transactions 1984;27(3):252–8.
[8] Willermet PA, Dailey DP, Carter Iii RO, Schmitz PJ, Zhu W. Mechanism of formation of antiwear films from zinc dialkyldithiophosphates. Tribol Int 1995;28 (3):177–87.
[9] Nicholls MA, Do T, Norton PR, Kasrai M, Bancroft GM. Review of the lubrication of metallic surfaces by zinc dialkyl-dithiophosphates. Tribol Int 2005;38(1):15–39.
[10] Aktary M, McDermott MT, McAlpine GA. Morphology and nanomechanical properties of ZDDP antiwear films as a function of tribological contact time. Tribol Lett 2002;12(3):155–62.
[11] Nicholls MA, Do T, Norton PR, Bancroft GM, Kasrai M, Capehart TW, Cheng YT, Perry T. Chemical and mechanical properties of ZDDP antiwear films on steel and thermal spray coatings studied by XANES spectroscopy and nanoindentation techniques. Tribol Lett 2003;15(3):241–8.
[12] Pereira G, Munoz-Paniagua D, Lachenwitzer A, Kasrai M, Norton PR, Capehart TW, Perry TA, Cheng YT. A variable temperature mechanical analysis of ZDDP-derived antiwear films formed on 52100 steel. Wear 2007;262:461–70.
[13] Umer J, Morris N, Leighton M, Rahmani R, Howell-Smith S, Wild R, Rahnejat H. Asperity level tribological investigation of automotive bore material and coatings. Tribol Int 2018;117:131–40.
[14] Umer J, Morris N, Leighton M, Rahmani R, Balakrishnan S, Rahnejat H. Nano and microscale contact characteristics of tribofilms derived from fully formulated engine oil". Tribol Int 2019;131:620–30.
[15] Briscoe BJ, Evans DCB. The shear properties of Langmuir-Blodgett layers. Proc. Roy. Soc., Series A 1982;380(1779):389–407.
[16] Blodgett KB, Langmuir I. Built-up films of barium stearate and their optical properties. Phys Rev 1937;51(11):964.
[17] Chong WWF, Rahnejat H. Nanoscale friction as a function of activation energies. Surf Topogr 2015;3(4):044002.
[18] Ku IS, Chong WWF, Reddyhoff T, Rahnejat H. Frictional characteristics of molecular length ultra-thin boundary adsorbed films. Meccanica 2015;50(7): 1915–22.
[19] Spikes H, Tysoe W. On the commonality between theoretical models for fluid and solid friction, wear and tribochemistry. Tribol Lett 2015;59(1):21.
[20] Tomlinson GA. "A molecular theory of friction", the London, Edinburgh, and Dublin philosophical Magazine and. J Sci 1929;7(46):905–39.
[21] Eyring H. Viscosity, plasticity, and diffusion as examples of absolute reaction rates. J Chem Phys 1936;4(4):283–91.
[22] Furlong OJ, Manzi SJ, Martini A, Tysoe WT. Influence of potential shape on constant-force atomic-scale sliding friction models. Tribol Lett 2015;60(2):21.
[23] Ewen JP, Kannam SK, Todd BD, Dini D. Slip of alkanes confined between surfactant monolayers adsorbed on solid surfaces. Langmuir 2018;34(13):3864–73.
[24] Bouhacina T, Aime JP, Gauthier S, Michel D, Heroguez V. Tribological behavior of a polymer grafted on silanized silica probed with a nanotip. Phys Rev B 1997;56 (12):7694.
[25] Müser MH. Velocity dependence of kinetic friction in the Prandtl-Tomlinson model. Phys Rev B 2011;84(12):125419.
[26] Fusco C, Fasolino A. Velocity dependence of atomic-scale friction: a comparative study of the one-and two-dimensional Tomlinson model. Phys Rev B 2005;71(4): 045413.
[27] Bradley RS. "The cohesive force between solid surfaces and the surface energy of solids", the London, Edinburgh, and Dublin Philosophical Magazine and. J Sci 1932;13(86):853–62.
[28] Derjaguin BV, Muller VM, Toporov YP. Effect of contact deformations on the adhesion of particles. J Colloid Interface Sci 1975;53(2):314–26.
[29] Johnson KL, Kendall K, Roberts AD. Surface energy and the contact of elastic solids. Proc. Roy. Soc., Series A 1971;324(1558):301–13.
[30] Maugis D. Adhesion of spheres: the JKR-DMT transition using a Dugdale model. J Colloid Interface Sci 1992;150(1):243–69.
[31] Hertz H. On the contact of elastic solids. Z. Reine Angew. Mathematik 1881;92: 156–71.
[32] Johnson KL, Greenwood JA. An adhesion map for the contact of elastic spheres. J Colloid Interface Sci 1997 Aug 15;192(2):326–33.
[33] Jacobs TD, Lefever JA, Carpick RW. A technique for the experimental determination of the length and strength of adhesive interactions between effectively rigid materials. Tribol Lett 2015;59(1):1.
[34] Gohar R, Rahnejat H. Fundamentals of tribology. London: Imperial College Press; 2008.
[35] Hamdan SH, Chong WWF, Ng JH, Chong CT, Zhang H. Nano-tribological characterisation of palm oil-based trimethylolpropane ester for application as boundary lubricant. Tribol Int 2018;127(1):1–9.
[36] Spikes H. Stress-augmented thermal activation: tribology feels the force. Friction 2018;6(1):1–31.
[37] Hirst W, Moore AJ. Elastohydrodynamic lubrication at high pressures II. Non-Newtonian behaviour. Proc R Soc A Math Phys Eng Sci 1979;365(1723):537–65.
[38] Bhushan B, editor. Handbook of nanotechnology. second ed. Columbus, OH, USA: Springer; 2017.
[39] He M, Blum AS, Overney G, Overney RM. Effect of interfacial liquid structuring on the coherence length in nanolubrication. Phys Rev Lett 2002;88(15):154302.
[40] Briscoe BJ, Tabor D. Shear properties of thin polymeric films. J Adhes 1978;9(2): 145–55.
[41] Morris N, Leighton M, De la Cruz M, Rahmani R, Rahnejat H, Howell-Smith S. Combined numerical and experimental investigation of the micro-hydrodynamics of chevron-based textured patterns influencing conjunctional friction of sliding contacts. Proc. IMechE, Part J: J. Engineering Tribology 2015;229(4):316–35.
[42] Gore M, Morris N, Rahmani R, Rahnejat H, King PD, Howell-Smith S. "A combined analytical-experimental investigation of friction in cylinder liner inserts under mixed and boundary regimes of lubrication". Lubr Sci 2017;29(5):293–316.
[43] Ruan JA, Bhushan B. "Atomic-scale friction measurements using friction force microscopy: part I—general principles and new measurement techniques". Trans. ASME, J. Tribology 1994;116(2):378–88.
[44] Carpick RW, Agrait N, Ogletree DF, Salmeron M. Measurement of interfacial shear (friction) with an ultrahigh vacuum atomic force microscope. J Vac Sci Technol B: Microelectronics and Nanometer Structures Processing, Measurement, and Phenomena 1996;14(2):1289–95.
[45] Carpick RW, Agrait N, Ogletree DF, Salmeron M. Variation of the interfacial shear strength and adhesion of a nanometer-sized contact. Langmuir 1996;12(13): 3334–40.
[46] Landman U, Luedtke WD, Nitzan A. Dynamics of tip-substrate interactions in atomic force microscopy. Surf Sci Lett 1989;210(3):L177–84.
[47] Chong WWF, Teodorescu M, Rahnejat H. Nanoscale elastoplastic adhesion of wet asperities. Proc. IMechE, Part J: J. Engineering Tribology 2013;227(9):996–1010.
[48] Campen S, Green JH, Lamb GD, Spikes HA. In situ study of model organic friction modifiers using liquid cell AFM; saturated and mono-unsaturated carboxylic acids. Tribol Lett 2015;57(2):18.
[49] Buenviaje CK, Ge S-R, Rafaillovich MH, Overney RM. Atomic force microscopy calibration methods for lateral force, elasticity, and viscosity. Proc. Mater. Res. Soc. Symp. 1998;522:187–92.
[50] Styles G, Rahmani R, Rahnejat H, Fitzsimons B. "In-cycle and life-time friction transience in piston ring–liner conjunction under mixed regime of lubrication". Int J Engine Res 2014;15(7):862–76.
[51] Leighton M, Nicholls T, De la Cruz M, Rahmani R, Rahnejat H. "Combined lubricant–surface system perspective: multi-scale numerical–experimental investigation". Proc Inst Mech Eng J J Eng Tribol 2017;231(7):910–24.
[52] Pereira G, Lachenwitzer A, Kasrai M, Bancroft GM, Norton PR, Abrecht M, Gilbert PUPA, Regier T, Blyth RIR, Thompson J. "Chemical and mechanical analysis of tribofilms from fully formulated oils Part 1–Films on 52100 steel". Tribol Mater Surf Interfaces 2007;1(1):48–61.
[53] Cizaire L, Martin JM, Gresser E, Dinh NT, Heau C. Tribochemistry of overbased calcium detergents studied by ToF-SIMS and other surface analyses. Tribol Lett 2004;17(4):715–21.
[54] Kapsa P, Martin JM, Blanc C, Georges JM. Antiwear mechanism of ZDDP in the presence of calcium sulfonate detergent. J Tribol 1981;103(4):486.
[55] Kasrai M, Fuller MS, Bancroft GM, Ryason PR. X-ray absorption study of the effect of calcium sulfonate on antiwear film formation generated from neutral and basic ZDDPs: Part 1—phosphorus species. Tribol Trans 2003;46(4):534–42.
[56] Bhushan B, Israelachvili JN, Landman U. Nanotribology: friction, wear and lubrication at the atomic scale. Nature 1995;374(6523):607.
[57] Martin JM. Antiwear mechanisms of zinc dithiophosphate: a chemical hardness approach. Tribol Lett 1999;6(1):1–8.
[58] Spikes HA. The history and mechanisms of ZDDP. Tribol Lett 2004;17(3):469–89.
[59] Krasowska M, Popescu MN, Ralston J. Hydrodynamics in nanoscale confinement: SFA and colloid probe AFM liquid drainage experiments. J Phys Conf Ser 2012;392 (1):012009.